HHS Public Access

Author manuscript

Neuron. Author manuscript; available in PMC 2022 March 17.

Published in final edited form as:

Neuron. 2021 March 17; 109(6): 971–983.e5. doi:10.1016/j.neuron.2021.01.007.

Interneuronal exchange and functional integration of synaptobrevin via extracellular vesicles

A. Alejandro Vilcaes[1,2,3,*], **Natali L. Chanaday**[3,†,*], **Ege T. Kavalali**[3,4,†]

[1]CONICET. Universidad Nacional de Córdoba. Centro de Investigaciones en Química Biológica de Córdoba (CIQUIBIC), Córdoba X5000HUA, Argentina.

[2]Universidad Nacional de Córdoba. Facultad de Ciencias Químicas. Departamento de Química Biológica Ranwel Caputto, Córdoba X5000HUA, Argentina.

[3]Department of Pharmacology, Vanderbilt University, Nashville, TN 37240-7933, USA

[4]Vanderbilt Brain Institute, Vanderbilt University, Nashville, TN 37232-2050, USA

Summary

Recent studies have investigated the composition and functional effects of extracellular vesicles secreted by variety of cell types. However, the mechanisms underlying the impact of these vesicles on neurotransmission remain unclear. Here, we isolated extracellular vesicles secreted by rat and mouse hippocampal neurons and found that they contain synaptic vesicle-associated proteins, in particular the vesicular SNARE (soluble NSF-attachment protein receptor) synaptobrevin (also called VAMP). Using a combination of electrophysiology and live-fluorescence imaging, we demonstrate that this extracellular pool of synaptobrevins can rapidly integrate into the synaptic vesicle cycle of host neurons via a CD81-dependent process and selectively augment inhibitory neurotransmission as well as specifically rescue neurotransmission in synapses deficient in synaptobrevin. These findings uncover a novel means of interneuronal communication and functional coupling via exchange of vesicular SNAREs.

In Brief

Vilcaes et al. uncover a novel form of interneuron communication using extracellular vesicles that allows the exchange of synaptic vesicle proteins, including synaptobrevin, via a CD81-dependent mechanism. Through this mechanism neurons can modify the protein composition and signaling properties of other neurons.

[†]Corresponding authors: natali.chanaday@vanderbilt.edu, ege.kavalali@vanderbilt.edu.
[*]These authors contributed equally to this work
Lead Contact: Ege T. Kavalali, Ph.D., Department of Pharmacology, Vanderbilt University, 465 21st Avenue South, 7130A MRBIII, PMB407933 Nashville, TN 37240-7933, phone: 615-343-5480

Author contribution

Conceptualization: NLC, AAV and ETK. Methodology, investigation, formal analysis: NLC and AAV. Interpretation, discussion, writing and editing: NLC, AAV and ETK. Funding and resources: ETK and NLC.

Declaration of interest

The authors declare no competing interests.

Keywords

Extracellular vesicles; neurotransmission; synaptic vesicle; synaptobrevin-2; CD81

Introduction

Extracellular vesicles (EVs) can be secreted by virtually any known cell type (van Niel et al., 2018). Initially believed to be a means for cells to eliminate waste materials, EVs have more recently been found to mediate inter-cellular signaling in healthy as well as pathological contexts (Kalluri and LeBleu, 2020). Extracellular vesicles constitute a rich substrate for the secretion of membranous proteins and lipids, which cannot be released via classical regulated exocytosis. In the nervous system, these secreted vesicles can impact a broad variety of normal and disease related processes including neuronal development, neurotransmission, regeneration and neurodegeneration (Antonucci et al., 2012; Budnik et al., 2016; Kawahara and Hanayama, 2018; Lachenal et al., 2011). Advances have been made in the last few years regarding the presence and role of secreted vesicles in the central nervous system, nevertheless the mechanism underlying EVs impact on neurotransmission remains unexplored. Here, by using a combination of proteomics, electrophysiology and live imaging, we uncover a novel pathway of interneuron communication by which neurons can modulate the release of neurotransmitters from other neurons.

Results

We isolated EVs from the media of astrocyte-free hippocampal neuron cultures (Figure S1A–B) via three different methods (Figure 1A). After a shared clearing procedure (Figure 1A, top), EVs were isolated by ultracentrifugation ((Théry et al., 2006); method 1), size exclusion chromatography (qEV Exosome Isolation from IZON; method 2) or using an affinity column (exoEasy Maxi Kit from QIAGEN; method 3). To characterize the EVs obtained with each method, we measured particle sizes and morphology by nanoparticle tracking analysis (NTA; Figure 1B) and transmission electron microscopy, respectively (TEM; insets in Figure 1B). The three methods yielded a similar size of EVs with a peak around 90 nm by NTA (Figure 1B). Accordingly, TEM images revealed that diameters of isolated EVs ranged around 90 nm, consistent with the size and morphology of EVs released by other cell types (Bachurski et al., 2019; Kibria et al., 2016; Koles et al., 2012; Sinha et al., 2016). Thus, the three methods tested here isolate a similar population of EVs from hippocampal neurons. To further characterize the identity of the EVs we performed a proteomics analysis (samples obtained using method 1; Figure 1C). A large number of the total proteins identified in our population of EVs were previously reported to be present in EVs (compared to Vesiclepedia - http://microvesicles.org/ - database). The majority of molecules comprised families of proteins previously found in secreted vesicles from different cell types and species (Choi et al., 2015; Koles et al., 2012; Kowal et al., 2016), including proteins related to the extracellular matrix, cell adhesion (ligands and receptors), different signaling molecules, metabolism (nucleic acids related, fatty acids related, chaperones and proteasome), and trafficking (secretion related, multi vesicular bodies biogenesis, endocytosis) (Figure 1C and Table S1). Classical EV markers were identified

(see (Choi et al., 2015)), including CD81, CD9, flotillin-1, fibronectin, annexin, ESCRT-1, TSG101, Hist1h4h, HSP70, VCP (CDC48) and ALIX (but not CD63; see full list of protein in Table S1). Consistent with this finding, confocal immunofluorescence analysis of localization revealed that CD81 is present in neurons and, in particular, in axons and presynaptic terminals (Figure S1C–G). In comparison, CD63 localized less to axons than CD81 (Figure S1H–K). The endoplasmic reticulum proteins GP96 and endoplasmin, as well as the *cis*-Golgi protein GM130, that are characteristically absent in EVs (Kowal et al., 2016) were also undetected in our samples. Besides the classical markers, the proteomics assay of EVs also revealed the presence of several neuronal proteins (Figure 1C) including neuron specific adhesion and signaling molecules, ion channels and synaptic vesicle proteins, among others (Figure 1C). In particular, N-ethylmaleimide-sensitive factor (NSF)-attachment factor receptor (SNARE) proteins associated with synaptic vesicle fusion, synaptobrevin-2 (syb2 or VAMP2), syntaxin-1A, as well as synaptoptagmin-5 (also called synaptotagmin-9) (Table S1) were found, with syb2 being the most abundant. Interestingly, the presence of SNARE proteins in EVs was previously shown to mediate a specific type of trans-synaptic communication that regulates synaptic plasticity at the *Drosophila* neuromuscular junction (Korkut et al., 2013). Contamination by synaptic vesicles can be excluded since classical markers including vesicular neurotransmitter transporters (VGLUT, VGAT, VMAT) and synapsin-1 were not detected in our preparation of EVs. Proteins of astrocytic origin were also largely absent from the EVs proteome. Taken together, our results support a predominantly neuronal origin of the secreted vesicles analyzed in this report.

Tetraspanins are a family of highly conserved proteins that regulate membrane morphology and dynamics affecting intracellular trafficking, exocytosis and endocytosis, cell motility and intercellular signaling (Hemler, 2005), but their role in neurotransmission remains unexplored. Tetraspanins are also found in EVs and used as markers (Choi et al., 2015). Among them, CD81 is one of the most studied member and its crystal structure was recently described (Zimmerman et al., 2016). We identified tetraspanin CD81 as a component of the EVs secreted by hippocampal neurons. Moreover, we also detected endogenous production CD81 in neurons, with ~50% of CD81 signal localizing to axons and presynaptic terminals (Figure 2A and Figure S1C–G), suggesting that CD81 may play a role in neurotransmission. To test this premise, we reduced the levels of CD81 in hippocampal neurons using a specific shRNA (CD81 knock down - KD - ; Figure 2B) or increased the protein levels of CD81 by overexpression (CD81 OE). Knocking down CD81 led to a decrease in miniature (i.e. spontaneous) inhibitory postsynaptic currents (mIPSC) frequency (Figure 2C–D), a phenotype that can be rescued by expressing shRNA-resistant CD81 (Figure 2C–D). Conversely, overexpression of CD81 caused an increase in the frequency of spontaneous inhibitory release (Figure 2C–D), suggesting that CD81 may modulate release of inhibitory neurotransmitters. Both human (Figure 2C–D) and rat (Figure S2A) CD81 had the same effect, as well as fluorescently labeled CD81 expression (Figure S2A). Moreover, expression of fluorescently tagged CD63, a protein that was undetected (i.e. below the limit of detection) in our proteomics analysis of EVs, had no impact on mIPSCs (Figure S2A). Accordingly, CD63 localizes less to axons and presynaptic terminals than CD81 (Figure S1H–K). Knocking down CD81 had no effect on excitatory spontaneous neurotransmission (or miniature excitatory postsynaptic currents, mEPSC; L307 infected control: frequency

2.3±0.2 Hz, amplitude 27±2 pA; CD81 KD: frequency 2.6±0.3 Hz, amplitude 23±2 pA). These results strongly support a specific role for tetraspanin CD81 in the regulation of inhibitory neurotransmission. Recently, a structural simulation analysis of CD81 revealed that cholesterol binding regulates the transition from an open to a close conformation, which was speculated to modulate CD81 interaction with other proteins and/or subcellular localization (Zimmerman et al., 2016). Thus, we next mutated two key residues in CD81 that were shown to abrogate cholesterol binding (CD81 E219A and CD81 E219Q) (Zimmerman et al., 2016). Overexpression of these mutants in wild-type hippocampal neurons had a dominant negative effect leading to a reduction in the frequency of mIPSCs, similar to the effect of CD81 KD (Figure 2C–D). The amplitude of mIPSC was similar for all experimental groups (Figure 2E and Figure S2B). Our results reveal CD81, a biomolecule involved in specific aspects of membrane trafficking and EV biology (Andreu and Yáñez-Mó, 2014; Charrin et al., 2014), as an endogenous regulator of inhibitory neurotransmitter release. These findings suggest that the synaptic vesicle cycle and the extracellular vesicle pathways may be interconnected.

We next asked whether EVs secreted by hippocampal neurons have any functional impact on synaptic vesicle release and neurotransmission. We recorded mIPSCs at different time points after wash out of the culture media with Tyrode's modified buffer and posterior addition of EVs (Figure 3A). EVs isolated by the three methods (3×10^8 particles/ml) equally caused a gradual increase in the frequency, but not the amplitude, of mIPSCs (Figure 3B–D), with a significant effect after 30 min post EVs addition when compared to untreated neurons (control, which have a stable mIPSC frequency in time; Figure 3B–D). This effect of EVs on mIPSC frequency was dose-dependent, with higher concentrations leading to a faster and more pronounced effect (Figure S2C–E). The estimated concentration of EVs in the culture media of hippocampal neurons is approximately 6×10^8 particles/ml (back calculated from the three EVs isolation methods; Figure S2F), so we chose 3×10^8 particles/ml concentration for all remaining experiments. Interestingly, neurons stimulated with 45 mM KCl for 10 min released a similar amount of EVs as unstimulated controls, suggesting that secretion of EVs is independent of activity in these acute conditions (Figure S2G). We then recorded miniature excitatory postsynaptic currents (mEPSC) using the same experimental setting and found that EVs addition had no impact on either frequency or amplitude of mEPSCs (Figure S2H–J). This is not due to selectivity in the uptake of EVs by excitatory or inhibitory neurons, since EVs labeled with syb2-pHluorin (see below) are incorporated to the same extent by VGluT1 and VGAT positive presynaptic boutons (Figure S3A–B). The experiments were performed in the presence of the action potential blocker tetrodotoxin (TTX). When neurons were incubated with EVs in the absence of TTX (allowing basal activity) the increase in frequency of mIPSC was similar to what was observed for EVs added in TTX, pointing to a more constitutive or activity-independent uptake mechanism of EVs (Figure 3E–G). Nevertheless, the increase in inhibitory neurotransmission mediated by EVs is calcium-dependent, since it is abrogated by the fast calcium buffer BAPTA-AM (Figure 3E–G). To test if proteinaceous components of EVs mediate the modulation of mIPSC, EVs were exposed to heat denaturation to inactivate proteins present in the vesicles (Chen et al., 2019; Ratajczak et al., 2006) and no impact on mIPSC frequency or amplitude were observed (Figure S3C–E), indicating that proteinaceous components of the EVs

mediate the effect on neurotransmission. In agreement, the modulation of neurotransmitter release is limited to EVs of neuronal origin since EVs isolated from cultured astrocytes (which may have a different composition) have no effect on either the frequency or the amplitude of mIPSCs (Figure 3H). Taken together, our results point to a specific role of EVs secreted by neurons in the modulation of calcium-dependent spontaneous inhibitory neurotransmission.

We next explored the role of CD81 in the regulation of mIPSCs by EVs. Secreted vesicles were isolated from neurons that lack CD81 (CD81 KD) and were found to have no effect on mIPSC frequency or amplitude when added to wild type (control) cultures (Figure 3B–D), indicating a key role for this protein in the regulation of inhibitory spontaneous neurotransmission by EVs. Moreover, EVs isolated from wild type neurons can rescue the reduction in mIPSC frequency observed in CD81 KD neurons (Figure S3F–H), suggesting that reincorporation of this protein can improve the synaptic defects. The concentration of secreted EVs into the culture media from CD81 KD neurons were similar to control (Figure S2F), therefore release of EVs is not affected by deletion of CD81. Tetraspanins, including CD81, can regulate cargo selection and sorting to EVs (Andreu and Yáñez-Mó, 2014). Thus, our findings suggest that knocking down CD81 may alter the protein composition of neuronal EVs impairing their effect on the target neuron.

So far we have identified a role for EVs of neuronal origin in the modulation of inhibitory spontaneous neurotransmitter release that is dependent on the tetraspanin CD81. We next assessed the impact of EVs on evoked, i.e. action potential mediated, inhibitory neurotransmission. The addition of EVs had no significant effect on the paired-pulse ratio or the amplitude of eIPSC (Figure S3I–K). We then stimulated at high frequency (20 Hz) to deplete the readily releasable pool of synaptic vesicles and mobilize the whole recycling pool. This stimulation revealed a higher rate of depression of evoked inhibitory neurotransmission after 30 to 60 min treatment with EVs (Figure S3L), with a 40–50% decrease in the amplitude of eIPSCs compared to control after the 4^{th} stimulation (inset in Figure S3L). This result indicates that EVs can increase to some extent the probability of release of synaptic vesicles, however, this effect is small such that it is undetected by paired-pulse ratio measurements but can become evident after high frequency stimulation. Taken together with our previous results, our data shows that EVs produced and secreted by neurons modulate specifically inhibitory spontaneous release of neurotransmitters and evoked probability of release. The presence of CD81 and cholesterol binding by CD81 seem to be crucial for this function.

In order to modulate neurotransmitter release, EVs may be affecting the molecules involved in synaptic vesicle exocytosis. Synaptic vesicle fusion is catalyzed by a highly specialized fusion machinery composed of neuronal SNARE proteins (Chanaday and Kavalali, 2018; Südhof, 2013). The most abundant synaptic vesicle SNARE is syb2 (Takamori et al., 2006). Even though a few copies of syb2 seem to be sufficient to trigger fusion (Sinha et al., 2011), increasing the number of SNAREs has been proposed to increase release probability and accelerate the fusion process (Acuna et al., 2014; Wu et al., 2017). Syb2 was present in EVs as determined by our proteomics analysis (Table S1). Therefore, we asked whether syb2 from EVs can be incorporated into synaptic vesicles at the target neuron. We first isolated

EVs from cultured hippocampal neurons expressing syb2 fused to the pH sensitive GFP, pHluorin. EVs obtained from these cultures emit green fluorescence that can be quenched by changing the pH of the solution from 7.4 to 5 (Figure S4A–B), but changing the pH from 7.4 to ~9 does not further increase the detection of fluorescent particles (Figure S4B), indicating that the EVs contain syb2-pHluorin and that the C-terminus (intraluminal in synaptic vesicles) region of syb2 is oriented towards the outside of the EVs (similar to syb2 orientation at the plasma membrane; Figure S4C). We next incubated wild type neurons with these syb2-pHluorin EVs and performed live imaging experiments at different times after EVs addition (Figure 4A). At the end of the experiment we either fixed the cells for immunofluorescence (Figure 4B) or perfused 50 mM NH_4Cl to reveal all pHluorin molecules (Figure 4C). For the immunodetection of incorporated syb2-pHluorin an anti-GFP antibody was used, and anti-synapsin 1 was used to label presynaptic terminals. Object-based colocalization analysis of confocal images revealed that syb2-pHluorin was incorporated by ~20% of neurons (Figure 4B) and present in cell bodies, axons and dendrites. In average, 3.8% of all synapsin 1 presynaptic boutons per field were positive for GFP (Figure 4B), suggesting that exogenous syb2-pHluorin from the EVs was incorporated and transported to presynaptic terminals. We are likely underestimating the number of presynaptic terminals and neurons incorporating syb2-pHluorin since regions presenting only a few molecules may not be detected by immunofluorescence. The fluorescence of pHluorin is quenched at acidic environments, as in the lumen of numerous trafficking organelles. Thus NH_4Cl is used to alkalinize all organelles and reveal pHlourins present in intracellular compartments. After 50–60 min of incubation with EVs containing syb2-pHluorin, perfusion of 50 mM NH_4Cl increased the basal fluorescence in bouton-like regions that resembled *en passant* synapses (Figure 4C). These results suggest that syb2 from EVs can be incorporated by the target neuron and transported to presynaptic terminals. To assess the functionality of the exogenous, newly incorporated syb2, we stimulated the neuronal network at high frequency (40 Hz 5 s) to mobilize the recycling pool of synaptic vesicles (Figure 4D). The boutons that responded showed a peak in fluorescence follow by a decay (Figure 4E), indicating possible fusion and endocytosis of syb2-pHluorin. The trafficking of syb2-pHluorin is evident in the ensemble (global) average peak (4 independent experiments; Figure 4E, bottom). Spots that showed basal fluorescence (background fluorescence), on the contrary, had no response to the stimulation and only underwent photobleaching (Figure 4E). These results strongly support that exogenous syb2 from EVs can be incorporated to synaptic vesicles and recycle in response to neuronal activity. Incorporation of syb2-pHluorin onto target neurons is severely reduced in CD81 KD EVs (Figure 4F–G, compare with 4B), in agreement with our previous results implicating a key role of CD81 in the EVs-mediated augmentation of neurotransmission. The amplitude distribution of syb2-pHluorin peaks showed a lognormal distribution (Figure 4E, inset) implying that the number of syb2-pHluorin molecules present in each presynaptic bouton and synaptic vesicle is random. In other words, the putative transport of exogenous syb2-pHluorin and intermixing with the endogenous pool may be a stochastic process. Accordingly, the rise time of fluorescence is correlated with the amplitude (Figure S4D), suggesting that higher amplitude peaks result from synapses where a higher number of vesicles containing syb2-pHluorin were fused. If synaptic vesicles containing syb2-pHluorin from EVs were indistinguishable from “dark” (non-fluorescent) synaptic vesicles, then they

would fuse randomly at any time point during the stimulation window. However, we observed an average peak rise time of 2 s (Figure S4E–F) suggesting that the extra syb2-pHluorin molecules incorporated may be conferring synaptic vesicles a slightly faster release propensity. That is, synaptic vesicles containing syb2-pHluorin are more prone to fuse and release their content (and undergo the concurrent endocytosis) before “dark” vesicles. This premise agrees with the increase in spontaneous release of inhibitory neurotransmitters (Figure 3B–D) and the faster depression in neurotransmission during high frequency stimulation caused by EVs treatment (Figure S3L).

To further test the ability of syb2 transported via EVs to be incorporated into the synaptic vesicle cycle, we investigated whether EVs can rescue neurotransmission in syb2 knock out (KO) neurons. Both, evoked and spontaneous neurotransmission are severely impaired in neurons lacking syb2 (Schoch et al., 2001). Following the same experimental design shown in Figure 3A, we incubated syb2 KO neurons with EVs isolated from wild type astrocyte-free hippocampal neuron cultures. Recordings from syb2 KO cultures showed the expected decrease in frequency of mIPSCs consistently for 1 hour, however the addition of EVs (3×10^8 particles/ml) increased the rate of spontaneous release with time partially reversing the phenotype (Figure 5A–B). The frequency of mIPSCs in syb2 KO neurons incubated with EVs reached values up to ~20% of the WT control frequency after 50–60 min incubation (inset in Figure 5B), a remarkable rescue given that only a modest number of presynaptic terminals incorporated exogenous syb2 (Figure 5B). mIPSC amplitudes in the syb2KO cultures were not affected by EVs (Figure 5C). This result demonstrates exogenously incorporated syb2 via EVs can rescue a considerable proportion of the spontaneous inhibitory neurotransmission in syb2 KO hippocampal neurons. Spontaneous excitatory neurotransmission can also be partially rescued by EVs in syb2 KO neurons (Figure 5D–E), agreeing with our previous findings of similar uptake of syb2-pHluorin from EVs by glutamatergic and GABAergic presynaptic terminals (Figure S3A–B). In addition, the previously described modulation of mIPSCs by CD81 (Figure 2C–E) also requires syb2, since CD81 does not increase mIPSC frequency in syb2 KO neurons (Figure S4G–I). While EVs isolated from wild type neurons contain syb2 (Figure 5F, and Figure 1C), EVs secreted by CD81 KD neurons do not contain detectable levels of syb2 (Figure 5F). When syb2-pHluorin is overexpressed, CD81 KD can also dramatically reduce the amount of syb2 in the EVs (Figure 5F). Taking together with our previous findings, these results provide strong evidence for CD81 regulating the recruitment of syb2 to EVs and thus it modulates neurotransmitter release via interneuronal exchange of syb2. Accordingly, EVs secreted from astrocytes, which had no effects on neurotransmission, have no detectable amounts of syb2 (Figure 5F).

Evoked inhibitory neurotransmission is greatly reduced in syb2 KO neurons (Figure 5G–H), but it cannot be rescued by addition of EVs (Figure 5G–H), possibly due to the small number of synapses and synaptic vesicles incorporating syb2 molecules as indicated by our previous experiments. We next isolated EVs from syb2 KO neurons and their littermate control, syb2 heterozygous mice (Het; Figure 5I). As previously shown for wild type EVs, EVs from syb2 heterozygous neurons increased the frequency of mIPSCs in syb2 KO neurons (Figure 5J–K). However, syb2 KO EVs had no impact on spontaneous inhibitory neurotransmission in either syb2 KO neuros (Figure 5J–K) or wild type neurons (Figure 5L),

supporting the premise that syb2 incorporation via EVs is necessary to increase synaptic vesicle release. Amplitudes of mIPSC were similar for all experimental groups (Figure 5M).

If the rescue of spontaneous neurotransmission is due to delivery of syb2, then EVs should not rescue the lack of other synaptic SNARE proteins that are not present in EVs (based on our proteomics analysis). To test this hypothesis, we used SNAP25 KO neurons which, similar to syb2 KO, have impaired spontaneous neurotransmission (Bronk et al., 2007). Incubation with EVs, which do not have detectable amounts of SNAP25, did not rescue spontaneous inhibitory neurotransmission in SNAP25 KO hippocampal neurons (Figure 6A–C). Syb2-pHluorin delivered via EVs cannot be exocytosed in response to electrical stimulation in SNAP25 KO neurons (Figure 6D), although syb2-pHluorin is incorporated by SNAP25 KO neurons and synapses similarly to wild type control neurons (Figure 6E–F). Thus, there is specificity of the synaptic vesicle proteins that EVs can deliver to neurons, which determines the effect they will have on neurotransmission.

Discussion

Our results demonstrate that exogenous synaptic vesicle proteins transported by extracellular vesicles can be incorporated into the synaptic vesicle cycle of target neurons (Figure 6H). In the past, molecular understanding of EVs secretion and incorporation by the target cell has been obscured by the use of complex samples (homogenized tissue or fluids) containing a mixture of diverse populations of EVs (Blanchette and Rodal, 2020; Budnik et al., 2016). Here we overcome this issue by isolating EVs from glia-free hippocampal neuron cultures. This population of EVs has a defined size of ~90 nm and contains classical EVs markers along with neuronal proteins, but not glial proteins, indicating a predominantly neuronal origin for the EVs. We show that these neuronal EVs can selectively augment inhibitory neurotransmitter release, both spontaneous and evoked, when incorporated by the target neuron. These findings reinforce the idea that the precise impact that EVs have on neurotransmission or, vice versa, the modulation of EVs levels by activity both depend on the identity of the secretory (i.e. neuron or glia) and of the target cell (Antonucci et al., 2012; Korkut et al., 2013; Lachenal et al., 2011). However, the underlying mechanism remains poorly understood. Our results reveal that the modulation of neurotransmission by EVs requires a proteinaceous machinery involving molecules that regulate the biology of EVs, such as the tetraspanin CD81, and molecules that drive the synaptic vesicle cycle and neurotransmitter release, such as the SNARE syb2. This exogenously delivered syb2 via EVs can be functionally incorporated into the synaptic vesicle cycle increasing the propensity to fuse of synaptic vesicles and it can partially rescue spontaneous neurotransmission in neurons from syb2 KO animals. CD81 is necessary for this syb2-mediated modulation, through regulating the recruitment of syb2 to EVs. Nevertheless, we cannot rule out a putative role for lipidic components of EVs (including cholesterol and sphingolipids; see (Antonucci et al., 2012; Kawahara and Hanayama, 2018; Wasser et al., 2007)), especially given the key role we found for cholesterol binding in CD81 function. Neuronal EVs, which do not contain SNAP25, cannot rescue neurotransmitter release in neurons lacking SNAP25. Moreover, astroglial EVs that lack syb2 have no impact on neurotransmission. These results indicate that there is specificity in the molecules that are

transported through EVs and this protein composition determines the effect EVs will have on neurotransmission.

Here we show that syb2-pHluorin, a commonly used fluorescent tool to monitor synaptic vesicle recycling, can be secreted by neurons via EVs. Taking advantage of this property, we could demonstrate that exogenous syb2-pHluorin can be incorporated into the synaptic vesicle cycle of the target neurons. This incorporation is independent of neuronal activity, since incubation with EVs in the presence or absence of TTX leads to comparable effects on neurotransmission and SNAP25 KO neurons can integrate syb2-pHluorin similarly to controls. The functional incorporation of syb2-pHluorin into the synaptic vesicle fusion machinery is supported by real-time monitoring of its trafficking (exocytosis and endocytosis) in response to electrical stimulation. EVs-delivered syb2-pHluorin requires its canonical partner SNAP25 to undergo exocytosis (since syb2-pHluorin cannot be exocytosed in SNAP25 KO neurons) and, furthermore, EV-mediated modulation of neurotransmitter release depends on calcium (as revealed by the fast calcium buffer BAPTA-AM), strengthening the notion that syb2 from EVs incorporates into functional SNAREs complexes and can drive synaptic vesicle fusion. In the short term, release of EVs is largely independent on neuronal activity, since acute elevated KCl incubation does not impact the levels of secreted EVs. Taken together, our findings point to the existence of a rather constitutive mechanism of secretion and incorporation of neuronal EVs. This is further supported by the fact that genetic manipulations, including overexpression and elimination of CD81 and/or syb2, do not lead to changes in secretion of EVs. However, we cannot exclude the possibility of long term modulation of EVs secretion in neurons by global activity levels (Lachenal et al., 2011).

Treatment of wild type neurons with EVs leads to selective augmentation of inhibitory, but not excitatory, neurotransmission suggesting that the underlying mechanism may differ among the two synapse types. However, syb2-pHluorin from EVs is equally incorporated by glutamatergic and GABAergic presynaptic terminals, indicating that another factor underlies the selectivity of effects. It was previously proposed for cerebellar and cortical neurons that syb2, along with other synaptic vesicle proteins, may be expressed at lower levels in GABAergic presynaptic boutons in comparison to glutamatergic counterparts (Benagiano et al., 2011; Bragina et al., 2010; but also see Grønborg et al., 2010). Therefore, a ceiling effect in excitatory synapses, where the endogenous high levels of syb2 occludes the effects of EVs, may underlie this discrepancy. Thus, removal of syb2 from excitatory synapses should lead to EV modulation of neurotransmission at these synapses. In agreement with this premise, we show that EVs can partially recue not only inhibitory, but also excitatory spontaneous neurotransmission in syb2 KO neurons, suggesting that the selectivity observed in wild type neurons may be due to variability in endogenous levels of syb2 among synapse types.

Our results indicate that the trafficking pathways of EV proteins and of synaptic vesicle molecules may be interconnected opening new avenues in the research of the molecular biology of EVs in neurons. This heretofore unknown mechanism may underlie a new form of interneuron communication by which one neuron impacts the protein composition and thus, the function of other neurons. Future experiments will be necessary to explore if

neurons can modify EVs protein composition in response to different stimuli such as long term activity, silencing, injury or neurodegeneration, and thus communicate their state to other neurons.

STAR Methods.

RESOURCE AVAILABILITY Lead Contact

Further information and requests for resources and reagents should be directed to and will be fulfilled by the Lead Contact, Ege T. Kavalali, Department of Pharmacology, Vanderbilt University, Nashville, TN 37240-7933, USA. Phone: 615-343-5480 ege.kavalali@vanderbilt.edu

Material Availability—All plasmids used in the present manuscript are available for sharing via request to ETK or AAV.

Data and Code Availability—This study did not generate any unique code. Custom scripts for pHluorin analysis are available through our previous publication (Chanaday and Kavalali, 2018). The authors are open to share any other material upon request to ETK or NLC.

Original/source data for Figure 1 (full list of proteomics results from hippocampal neuron extracellular vesicles) in the paper is available in supplemental Table S1.

EXPERIMENTAL MODEL AND SUBJECT DETAILS

Primary muse and rat hippocampal cultures—Dissociated hippocampal cultures from embryonic day 17–19 or postnatal day 0–2 Sprague-Dawley rats of both sexes were used for all the experiments. To prepare syb2 KO and SNAP25 KO cultures, embryonic day 17–19 mice of both sexes were used (Schoch et al., 2001).

All experiments were performed following protocols approved by the UT Southwestern Institutional Animal Care and Use Committee and the Vanderbilt University Medical Center Institutional Animal Care and Use Committee.

Sample size estimation—The approach we used for this research is hypothesis free, we did not have prior knowledge of the type of result or values we were going to obtain or of the magnitude of the effect of extracellular vesicles. For that reason, prior statistical power analysis and sample-size estimation was not possible. Nevertheless, the number of experiments and samples needed can be inferred from previous, similar experiments performed in our lab, using the same type of cultures. Assuming the reproducibility of experimental conditions and settings, we estimated that a minimum of 3 independent cultures with 2 coverslips (with ~10–30 presynaptic boutons per coverslip analyzed for live imaging experiments and ~3–6 whole cell recordings per coverslip for electrophysiology) per experimental group was enough for significance testing and finding the presence or absence of differences or tendencies among groups. Based on the variances and tendencies observed, in some cases the addition of extra experiments was decided.

Experimental groups were pre-designed based on the hypothesis (e.g. treated vs untreated control). All experimental groups for each particular data set were present in each experiment and measured in a random order under the exact same conditions (i.e. buffers, solutions, drugs and other reagents as well as temperature, culture age and other conditions were the same for all samples).

METHOD DETAILS

Dissociated hippocampal cultures—Bilateral hippocampi were dissociated using 10 mg/ml trypsin and 0.5 mg/ml DNAse for 10 min at 37°C. Tissue was carefully triturated using a P1000 pipette and cells were plated onto glass coverslips (for imaging and electrophysiology) or plastic bottom plates (for EVs isolation) previously coated with Matrigel. Basic growth medium consisted of MEM medium (no phenol red), 5 g/l D-glucose, 0.2 g/l NaHCO3, 100 mg/l transferrin, 5% of fetal bovine serum, 0.5 mM L-glutamine, 2% B-27 supplement, and 2–4 μM cytosine arabinoside. Cultures were kept in humidified incubators at 37°C and gassed with 95% air and 5% CO_2.

Special hippocampal cultures were performed to isolate Extracellular Vesicles (refer to Isolation of extracellular vesicles section).

Cloning and lentiviral infection—Previously described point mutations on CD81 (Zimmerman et al., 2016) were generated using a commercial kit and classic PCR techniques. The sequence of shRNA against CD81 (5’-GCACCAAATGCATCAAATATCAAGAGTATTTGATGCATTTGGTGC-3’) was inserted into L307 lentiviral vector (gift of Dr. Thomas C. Südhof, Stanford University). CD63-pHluorin was a generous gift of Dr. Alissa M. Weaver (Vanderbilt University Medical Center) (Sung et al., 2015). For CD81 constructs, the cDNA sequences NM_013087.2 (rat CD81, OriGene) and NM_004356.4 (human CD81, AddGene) were used. All constructs for protein expression were subcloned into pFU-GW lentiviral vector from Addgene (plasmid # 14883).

Lentiviruses were produced in HEK293T cells by contransfection of pFUGW vectors and 3 packaging plasmids (pCMV-VSV-G, pMDLg/pRRE, pRSV-Rev) using Fugene 6 transfection reagent. Fresh, cleared supernatants containing lentiviruses were used for infection of days in vitro (DIV) 4 hippocampal neurons.

All experiments were performed on 16–20 DIV cultures when synapses were mature and lentiviral expression of constructs of interest was optimal (Deák et al., 2006; Mozhayeva et al., 2002).

Isolation of extracellular vesicles—Hippocampal neurons from P0–P1 rats were cultured as previously described (Kavalali et al., 1999) with modifications to reduce glia content (Beaudoin et al., 2012; Brewer et al., 1993). 2 days after plating, cytosine arabinoside (Ara C; 1-β-D-arabinofuranosylcytosine) was added at a final concentration of 2 μM to inhibit the proliferation of dividing non-neuronal (glial) cells. Neurons were maintained in Neurobasal (Gibco) supplemented with 2% B27 (Gibco), 1 mM sodium pyruvate and 2 mM glutamine. Every 4th day, half the medium was discarded from each

dish and replaced with fresh maintenance medium warmed to 37 °C. Under these experimental conditions, the population of astrocytes is remarkably reduced (see Fig. S1 and reference (Brewer et al., 1993)). Immunostaining of 14 DIV cultures with a monoclonal antibody against GFAP, revealed staining of only 1 to 2% of total cells, demonstrating minimal contamination by astrocytes.

At DIV 12–14, we replaced half the medium from each dish with fresh maintenance medium warmed to 37 °C. Then, every 24 h we added 30% of freshly maintenance medium warmed to 37 °C. After 60 h, culture supernatant was collected and cleared by serial centrifugation at 300 × g for 10 min (to sediment live cells), 2.000 × g for 10 min (to remove dead cells) and 18000 × g for 30 min (to sediment debris and microvesicles). Then, the supernatant was filtered through a 0.45 μm syringe filter (low affinity for proteins, Catalogue # SFPES013045S, Wyvern Scientific). The resulting supernatant was used for EVs isolation by the different methods.

The classical ultracentrifugation method (UC, method 1) consisted of two rounds of centrifugation at 100,000 × g for 80 min at 8°C (Théry et al., 2006). For other commercial kits (qEVoriginal Exosome from IZON and exoEasy Maxi Kit from QIAGEN, methods 2 and 3, respectively), we followed the procedures suggested by their respective suppliers. The EVs were resuspended (UC), collected (qEV) or exchanged of buffers (QIAGEN) using the Amicon Ultra-0.5 device in Tyrode's modified buffer (see Electrophysiology section).

Proteomics—Purified exosome fractions were resuspended in Laemmli sample buffer, incubated at 95°C for 5 min, and loaded onto 10 % denaturing polyacrylamide protein gels (SDS-PAGE). Single gel lanes containing the purified EVs were picked out of the gels and digested overnight with trypsin (Promega) following reduction and alkylation with Dithiothreitol (DTT) and iodoacetamide (Sigma–Aldrich). The samples then underwent solid-phase extraction cleanup with an Oasis HLB plate (Waters) and the resulting samples were injected onto an Orbitrap Fusion Lumos mass spectrometer coupled to an Ultimate 3000 RSLC-Nano liquid chromatography system. Samples were injected onto a 75 μm i.d., 75-cm long EasySpray column (Thermo) and eluted with a gradient from 0–28% buffer B over 90 min. Buffer A contained 2% (v/v) ACN and 0.1% formic acid in water, and buffer B contained 80% (v/v) ACN, 10% (v/v) trifluoroethanol, and 0.1% formic acid in water. The mass spectrometer operated in positive ion mode with a source voltage of 2.2 kV and an ion transfer tube temperature of 275 °C. MS scans were acquired at 120,000 resolution in the Orbitrap and up to 10 MS/MS spectra were obtained in the ion trap for each full spectrum acquired using higher-energy collisional dissociation (HCD) for ions with charges 2–7. Dynamic exclusion was set for 25 s after an ion was selected for fragmentation.

Raw MS data files were analyzed using Proteome Discoverer v2.2 (Thermo), with peptide identification performed using Sequest HT searching against the Rattus Norvegicus protein database from UniProt. Fragment and precursor tolerances of 10 ppm and 0.6 Da were specified, and three missed cleavages were allowed. Carbamidomethylation of Cys was set as a fixed modification, with oxidation of Met set as a variable modification. The false-discovery rate (FDR) cutoff was 1% for all peptides.

Electron microscopy—Transmission electron microscopy (TEM) was carried out essentially as previously described (Higginbotham et al., 2016; Zhang et al., 2019). EVs were fixed with 2.5% glutaraldehyde in 0.1 M sodium cacodylate buffer for 40 min at RT. The samples were incubated on formvar carbon-coated grids for 1 min followed by negative staining with 2% uranyl acetate for 45 s. Imaging was performed on a Philips/FEI T-12 transmission electron microscope.

Nanoparticle tracking analysis—Nanoparticle Tracking Analysis A NS300 NTA machine (Malvern NanoSight NS300) was used to analyze isolated EVs. Following camera settings were used: camera level 15, screen gain 1.0, and threshold 5. NTA was performed by acquisition of 60 s videos by triplicate (>500 tracks per video) of a 1 ml sample in Tyrode's buffer (see Electrophysiology section). Room temperature was recorded manually and did not exceed 25°C. Calibrations were performed using polystyrene latex microspheres with sizes of 100, 200, and 400 nm.

Western blotting—Western blots were performed using our described method (Nosyreva and Kavalali, 2010). Primary antibodies against GDI1 and CD81 were used in 1:2000 and 1:1000 dilution, respectively. Near-infrared secondary antibodies and an Odyssey scanner (LI-COR) were used to detect immunoreactive bands. Images were analyzed using Fiji (NIH). CD81 protein levels were normalized to GDI1 loading control.

Dot-blot—EVs and brain homogenates were resuspended in Tyrode's buffer. $1.5*10^9$ EV particles were added in each well in a BioDot Microfiltration apparatus (Biorad). Protocol was performed following the manufacturer recommendations with minor modifications. Briefly, samples were allowed to filtrate through the nitrocellulose membrane over-night at 4 °C followed by blocking and antibody staining. Near-infrared secondary antibodies and an Odyssey scanner (LI-COR) were used to detect the target proteins.

Immunofluorescence, confocal microscopy and colocalization analysis—Neuron cultures were fixed with 1% para-formaldehyde (PFA) and 7.5% sucrose in phosphate buffered saline (PBS) and permeabilized using 0.0075% digitonin in PBS. After blocking (1% bovine serum albumin (BSA), 3% goat serum and 0.2% fish gelatin in PBS), primary and secondary antibodies were diluted in blocking buffer and incubated over-night at 4 °C in a humid chamber. Antibodies against Syn1 (1:2000) and Tau (1:500) were from Synaptic Systems. Anti-GFP (1:100) was from Cell Signaling. Antibodies against GFAP (1:1000), CD63 (1:500), CD81 (1:100) and Flot1 (1:1000) were from Abcam.

Confocal images were acquired using an LSM 510 META confocal microscope (Carl Zeiss) with a 63X (NA1.4) objective. Object-based colocalization was analyzed using Fiji (NIH). 3D objects in each channel were segmented and positive colocalization was defined as an overlap of more than 50 voxels of two colors in the same object (calibration: 1 voxel = 0.143 × 0.143 × 1 μm).

Electrophysiology—Whole cell recordings of pyramidal neurons were performed using Axopatch 200B and Clampex 8.0 software (Molecular Devices), filtering at 1 kHz and sampling at 5 kHz while clamping the voltage at −70 mV. The internal pipette solution

contained 115 mM $CsMeSO_3$, 10 mM CsCl, 5 mM NaCl, 10 mM HEPES, 0.6 mM EGTA, 20 mM tetraethylammonium chloride, 4 mM Mg-ATP, 0.3 mM Na_2GTP and 10 mM QX-314 (lidocaine N-ethyl bromide). The final solution was adjusted to pH 7.3 and 305–310 mOsM. Final resistance of the electrode tips was ~2–5 MΩ. Electrical stimulation to elicit evoked responses was delivered using a parallel bipolar electrode (FHC) and a constant current unit (WPI A385) with a Master-8 controller (A.M.P.I.). Pulse duration was 0.1 ms and intensity was 35 mA.

For all experiments, the extracellular solution was a modified Tyrode's solution containing 150 mM NaCl, 4 mM KCl, 10 mM glucose, 10 mM HEPES and 2 mM $MgCl_2$, adjusted to pH 7.4 and 315–320 mOsM. The agonists against ionotropic glutamate receptors 6-cyano-7-nitroquinoxaline-2,3-dione (CNQX, 10 μM) and aminophosphonopentanoic acid (AP-5, 50 μM) were used to isolate inhibitory postsynaptic currents. To isolate excitatory (AMPA-mediated) currents, the GABA-A receptor inhibitor picrotoxin (PTX, 50 μM) and AP-5 were added to the bath solution. Spontaneous neurotransmission was recorded with the addition of 1 μM TTX. Evoked recordings were analyzed using Clapfit (Molecular Devices) and miniature events were analyzed with MiniAnalysis (Synaptosoft).

Fluorescence live imaging—Cultured hippocampal neurons were imaged in the modified Tyrode's buffer from above. Fluorescence was recorded using a Nikon Eclipse TE2000-U microscope (Nikon) and an Andor iXon+ back-illuminated EMCCD camera (Model no. DU-897E-CSO-#BV). For illumination we used a Lambda-DG4 illumination system (Sutter instruments) with a FITC emission filter. Images were acquired at 5 Hz. Solutions were perfused using an automatic, constant flux system (AutoMate Scientific). Circular regions of interest (ROI) of 2 μm diameter were drawn around local fluorescence maxima (putative presynaptic boutons) and measured using Fiji (NIH). Fluorescence peaks synchronous respect to the stimulation were detected and analyzed using Matlab.

QUANTIFICATION AND STATISTICAL ANALYSIS

Detailed statistical information for each experiment is provided in the respective figure legends. Briefly, the Kolmogorov-Smirnov (K-S) test was used to determine differences in cumulative probability histograms when comparing 2 groups, for 3 or more groups histograms were compared using Kruskal-Wallis analysis of medians and Dunn's multiple comparison post-test. For parametrically-distributed data, t-test and one-way or two-way ANOVA with appropriate multiple comparison post-tests (Sidak or Tukey) were employed, depending on the number of groups and treatments. If a different test was employed the respective information is presented in the figure legends. Detailed N for each group and experiment are informed in the figure legends. Plotted data in the figures always inform mean values ± SEM unless otherwise stated in the legend. Effort was directed to minimize the number of animals used for the experiments.

Supplementary Material

Refer to Web version on PubMed Central for supplementary material.

Acknowledgements

We would like to thank Dr Hamid Mirzaei (UT Southwestern) for his help in performing and analyzing the proteomics experiment. We are grateful to Dr Evan Krystofiak from the Research Electron Microscropy Resource (Vanderbilt University) and Dr Dmitry S. Koktysh from VINSE Nanocrystal/Analytical Laboratory (Vanderbilt University) for their assistance. We are grateful to Dr Alissa Weaver for generously providing the CD63-pHluorin construct. We also thank Drs. Lisa Monteggia, Helmut Kramer, Alissa Weaver and Qiangjun Zhou for their insightful comments on the manuscript. This work was supported by a grant from the National Institute of Mental Health (MH066198) to ETK, by a research fellowship from the Scientific and Technical Research National Council of Argentina (CONICET) to AAV and a NARSAD young investigator award to NLC.

References

Acuna C, Guo Q, Burré J, Sharma M, Sun J, and Südhof TC (2014). Microsecond dissection of neurotransmitter release: SNARE-complex assembly dictates speed and Ca^{2+} sensitivity. Neuron 82, 1088–1100. [PubMed: 24908488]

Andreu Z, and Yáñez-Mó M (2014). Tetraspanins in extracellular vesicle formation and function. Front Immunol 5, 442. [PubMed: 25278937]

Antonucci F, Turola E, Riganti L, Caleo M, Gabrielli M, Perrotta C, Novellino L, Clementi E, Giussani P, Viani P, et al. (2012). Microvesicles released from microglia stimulate synaptic activity via enhanced sphingolipid metabolism. EMBO J 31, 1231–1240. [PubMed: 22246184]

Bachurski D, Schuldner M, Nguyen PH, Malz A, Reiners KS, Grenzi PC, Babatz F, Schauss AC, Hansen HP, Hallek M, and Pogge von Strandmann E (2019). Extracellular vesicle measurements with nanoparticle tracking analysis - An accuracy and repeatability comparison between NanoSight NS300 and ZetaView. J Extracell Vesicles 8, 1596016. [PubMed: 30988894]

Beaudoin GM, Lee SH, Singh D, Yuan Y, Ng YG, Reichardt LF, and Arikkath J (2012). Culturing pyramidal neurons from the early postnatal mouse hippocampus and cortex. Nat Protoc 7, 1741–1754. [PubMed: 22936216]

Benagiano V, Lorusso L, Flace P, Girolamo F, Rizzi A, Bosco L, Cagiano R, Nico B, Ribatti D and Ambrosi G (2011). VAMP-2, SNAP-25A/B and syntaxin-1 in glutamatergic and GABAergic synapses of the rat cerebellar cortex. BMC Neurosci 17, 12:118. [PubMed: 22094010]

Blanchette CR, and Rodal AA (2020). Mechanisms for biogenesis and release of neuronal extracellular vesicles. Curr Opin Neurobiol 63, 104–110. [PubMed: 32387925]

Bragina L, Giovedì S, Barbaresi P, Benfenati F and Conti F (2010). Heterogeneity of glutamatergic and GABAergic release machinery in cerebral cortex: analysis of synaptogyrin, vesicle-associated membrane protein, and syntaxin. Neuroscience 165(3), 934–943. [PubMed: 19909789]

Bodin S, Planchon D, Rios Morris E, Comunale F, and Gauthier-Rouvière C (2014). Flotillins in intercellular adhesion - from cellular physiology to human diseases. J Cell Sci 127, 5139–5147. [PubMed: 25413346]

Brewer GJ, Torricelli JR, Evege EK, and Price PJ (1993). Optimized survival of hippocampal neurons in B27-supplemented Neurobasal, a new serum-free medium combination. J Neurosci Res 35, 567–576. [PubMed: 8377226]

Bronk P, Deák F, Wilson MC, Liu X, Südhof TC, and Kavalali ET (2007). Differential effects of SNAP-25 deletion on Ca2+ -dependent and Ca2+ -independent neurotransmission. J Neurophysiol 98, 794–806. [PubMed: 17553942]

Budnik V, Ruiz-Cañada C, and Wendler F (2016). Extracellular vesicles round off communication in the nervous system. Nat Rev Neurosci 17, 160–172. [PubMed: 26891626]

Chanaday NL, and Kavalali ET (2018). Optical detection of three modes of endocytosis at hippocampal synapses. Elife 7.

Chanaday NL, and Kavalali ET (2018). Presynaptic origins of distinct modes of neurotransmitter release. Curr Opin Neurobiol 51, 119–126. [PubMed: 29597140]

Charrin S, Jouannet S, Boucheix C, and Rubinstein E (2014). Tetraspanins at a glance. J Cell Sci 127, 3641–3648. [PubMed: 25128561]

Chen J, Jin L, Yan M, Yang Z, Wang H, Geng S, Gong Z, and Liu G (2019). Serum Exosomes from Newborn Piglets Restrict Porcine Epidemic Diarrhea Virus Infection. J Proteome Res 18, 1939–1947. [PubMed: 30983354]

Choi DS, Kim DK, Kim YK, and Gho YS (2015). Proteomics of extracellular vesicles: Exosomes and ectosomes. Mass Spectrom Rev 34, 474–490. [PubMed: 24421117]

Deák F, Shin OH, Kavalali ET, and Südhof TC (2006). Structural determinants of synaptobrevin 2 function in synaptic vesicle fusion. J Neurosci 26, 6668–6676. [PubMed: 16793874]

Dull T, Zufferey R, Kelly M, Mandel RJ, Nguyen M, Trono D, & Naldini L (1998). A third-generation lentivirus vector with a conditional packaging system. Journal of virology, 72(11), 8463–8471. [PubMed: 9765382]

Grønborg M, Pavlos NJ, Brunk I, Chua JJE, Münster-Wandowski A, Riedel D, Ahnert-Hilger G, Urlaub H and Jahn R (2010). Quantitative comparison of glutamatergic and GABAergic synaptic vesicles unveils selectivity for few proteins including MAL2, a novel synaptic vesicle protein. J Neurosci 30(1), 2–12. [PubMed: 20053882]

Hemler ME (2005). Tetraspanin functions and associated microdomains. Nat Rev Mol Cell Biol 6, 801–811. [PubMed: 16314869]

Higginbotham JN, Zhang Q, Jeppesen DK, Scott AM, Manning HC, Ochieng J, Franklin JL, and Coffey RJ (2016). Identification and characterization of EGF receptor in individual exosomes by fluorescence-activated vesicle sorting. J Extracell Vesicles 5, 29254. [PubMed: 27345057]

Kalluri R, and LeBleu VS (2020). The biology. Science 367.

Kalra H, Simpson RJ, Ji H, Aikawa E, Altevogt P, Askenase P, Bond VC, Borras FE, Breakefield X, Budnik V, Buzas E, Camussi G, Clayton A, Cocucci E, Falcon-Perez JM, Gabrielsson S, Gho YS, Gupta D, Harsha HC, Hendrix A, Hill AF, Inaal JM, Jenster G, Kiang LS, Kramer-Albers E-M,Llorente A, Lotvall J, Mincheva-Nilsson L, Nazarenko I, Nieuwland R, Nolte-'t Hoen ENM, Pandey A, Patel T, Piper MG, Pluchino S, Prasad TSK, Rajendran L, Raposo G, Record M, Reid GE, Sanchez-Madrid F, Schiffelers RM, Siljander P, Stoorvogel W, Taylor D, Thery C, Valadi H, van Balkom BWM, Vazquez J, Vidal M, Yanez-Mo M, Zoeller M and Mathivanan S (2012) Vesiclepedia: A compendium for extracellular vesicles with continuous community annotation. PLoS Biology. 12, e1001450.

Kavalali ET, Klingauf J, and Tsien RW (1999). Activity-dependent regulation of synaptic clustering in a hippocampal culture system. Proc Natl Acad Sci U S A 96, 12893–12900. [PubMed: 10536019]

Kawahara H, and Hanayama R (2018). The Role of Exosomes/Extracellular Vesicles in Neural Signal Transduction. Biol Pharm Bull 41, 1119–1125. [PubMed: 30068858]

Kibria G, Ramos EK, Lee KE, Bedoyan S, Huang S, Samaeekia R, Athman JJ, Harding CV, Lötvall J, Harris L, et al. (2016). A rapid, automated surface protein profiling of single circulating exosomes in human blood. Sci Rep 6, 36502. [PubMed: 27819324]

Koles K, Nunnari J, Korkut C, Barria R, Brewer C, Li Y, Leszyk J, Zhang B, and Budnik V (2012). Mechanism of evenness interrupted (Evi)-exosome release at synaptic boutons. J Biol Chem 287, 16820–16834. [PubMed: 22437826]

Korkut C, Li Y, Koles K, Brewer C, Ashley J, Yoshihara M, and Budnik V (2013). Regulation of postsynaptic retrograde signaling by presynaptic exosome release. Neuron 77, 1039–1046. [PubMed: 23522040]

Kowal J, Arras G, Colombo M, Jouve M, Morath JP, Primdal-Bengtson B, Dingli F, Loew D, Tkach M, and Théry C (2016). Proteomic comparison defines novel markers to characterize heterogeneous populations of extracellular vesicle subtypes. Proc Natl Acad Sci U S A 113, E968–977. [PubMed: 26858453]

Kwiatkowska K, Matveichuk OV, Fronk J, and Ciesielska A (2020). Flotillins: At the Intersection of Protein. Int J Mol Sci 21.

Lachenal G, Pernet-Gallay K, Chivet M, Hemming FJ, Belly A, Bodon G, Blot B, Haase G, Goldberg Y, and Sadoul R (2011). Release of exosomes from differentiated neurons and its regulation by synaptic glutamatergic activity. Mol Cell Neurosci 46, 409–418. [PubMed: 21111824]

Mozhayeva MG, Sara Y, Liu X, and Kavalali ET (2002). Development of vesicle pools during maturation of hippocampal synapses. J Neurosci 22, 654–665. [PubMed: 11826095]

Nosyreva E, and Kavalali ET (2010). Activity-dependent augmentation of spontaneous neurotransmission during endoplasmic reticulum stress. J Neurosci 30, 7358–7368. [PubMed: 20505103]

Ramirez DM, Khvotchev M, Trauterman B, and Kavalali ET (2012). Vti1a identifies a vesicle pool that preferentially recycles at rest and maintains spontaneous neurotransmission. Neuron 73, 121–134. [PubMed: 22243751]

Ratajczak J, Wysoczynski M, Hayek F, Janowska-Wieczorek A, and Ratajczak MZ (2006). Membrane-derived microvesicles: important and underappreciated mediators of cell-to-cell communication. Leukemia 20, 1487–1495. [PubMed: 16791265]

Schindelin J, Arganda-Carreras I, Frise E, Kaynig V, Longair M, Pietzsch T, Preibisch S, Rueden C, Saalfeld S, Schmid B, et al. (2012). Fiji: an open-source platform for biological-image analysis. Nat Methods 9, 676–682. [PubMed: 22743772]

Schoch S, Deák F, Königstorfer A, Mozhayeva M, Sara Y, Südhof TC, and Kavalali ET (2001). SNARE function analyzed in synaptobrevin/VAMP knockout mice. Science 294, 1117–1122. [PubMed: 11691998]

Sinha R, Ahmed S, Jahn R, and Klingauf J (2011). Two synaptobrevin molecules are sufficient for vesicle fusion in central nervous system synapses. Proc Natl Acad Sci U S A 108, 14318–14323. [PubMed: 21844343]

Sinha S, Hoshino D, Hong NH, Kirkbride KC, Grega-Larson NE, Seiki M, Tyska MJ, and Weaver AM (2016). Cortactin promotes exosome secretion by controlling branched actin dynamics. J Cell Biol 214, 197–213. [PubMed: 27402952]

Stewart SA, Dykxhoorn DM, Palliser D, Mizuno H, Yu EY, An DS, Sabatini DM, Chen IS, Hahn WC, Sharp PA, Weinberg RA, & Novina CD (2003). Lentivirus-delivered stable gene silencing by RNAi in primary cells. RNA (New York, N.Y.), 9(4), 493–501.

Südhof TC (2013). Neurotransmitter release: the last millisecond in the life of a synaptic vesicle. Neuron 80, 675–690. [PubMed: 24183019]

Sung BH, Ketova T, Hoshino D, Zijlstra A, and Weaver AM (2015). Directional cell movement through tissues is controlled by exosome secretion. Nat Commun 6, 7164. [PubMed: 25968605]

Takamori S, Holt M, Stenius K, Lemke EA, Grønborg M, Riedel D, Urlaub H, Schenck S, Brügger B, Ringler P, et al. (2006). Molecular anatomy of a trafficking organelle. Cell 127, 831–846. [PubMed: 17110340]

Théry C, Amigorena S, Raposo G, and Clayton A (2006). Isolation and characterization of exosomes from cell culture supernatants and biological fluids. Curr Protoc Cell Biol Chapter 3, Unit 3.22.

van Niel G, D'Angelo G, and Raposo G (2018). Shedding light on the cell biology of extracellular vesicles. Nat Rev Mol Cell Biol 19, 213–228. [PubMed: 29339798]

Wasser CR, Ertunc M, Liu X, and Kavalali ET (2007). Cholesterol-dependent balance between evoked and spontaneous synaptic vesicle recycling. J Physiol 579, 413–429. [PubMed: 17170046]

Wu Z, Bello OD, Thiyagarajan S, Auclair SM, Vennekate W, Krishnakumar SS, O'Shaughnessy B, and Karatekin E (2017). Dilation of fusion pores by crowding of SNARE proteins. Elife 6.

Zhang Q, Higginbotham JN, Jeppesen DK, Yang YP, Li W, McKinley ET, Graves-Deal R, Ping J, Britain CM, Dorsett KA, et al. (2019). Transfer of Functional Cargo in Exomeres. Cell Rep 27, 940–954.e946. [PubMed: 30956133]

Zimmerman B, Kelly B, McMillan BJ, Seegar TCM, Dror RO, Kruse AC, and Blacklow SC (2016). Crystal Structure of a Full-Length Human Tetraspanin Reveals a Cholesterol-Binding Pocket. Cell 167, 1041–1051.e1011. [PubMed: 27881302]

Highlights

- Neuronal extracellular vesicles (EVs) augment neurotransmitter release
- Synaptobrevin-2 (syb2) is recruited to EVs via CD81
- Syb2 from EVs is incorporated into functional recycling synaptic vesicles
- EVs can rescue spontaneous neurotransmission in syb2 KO neurons

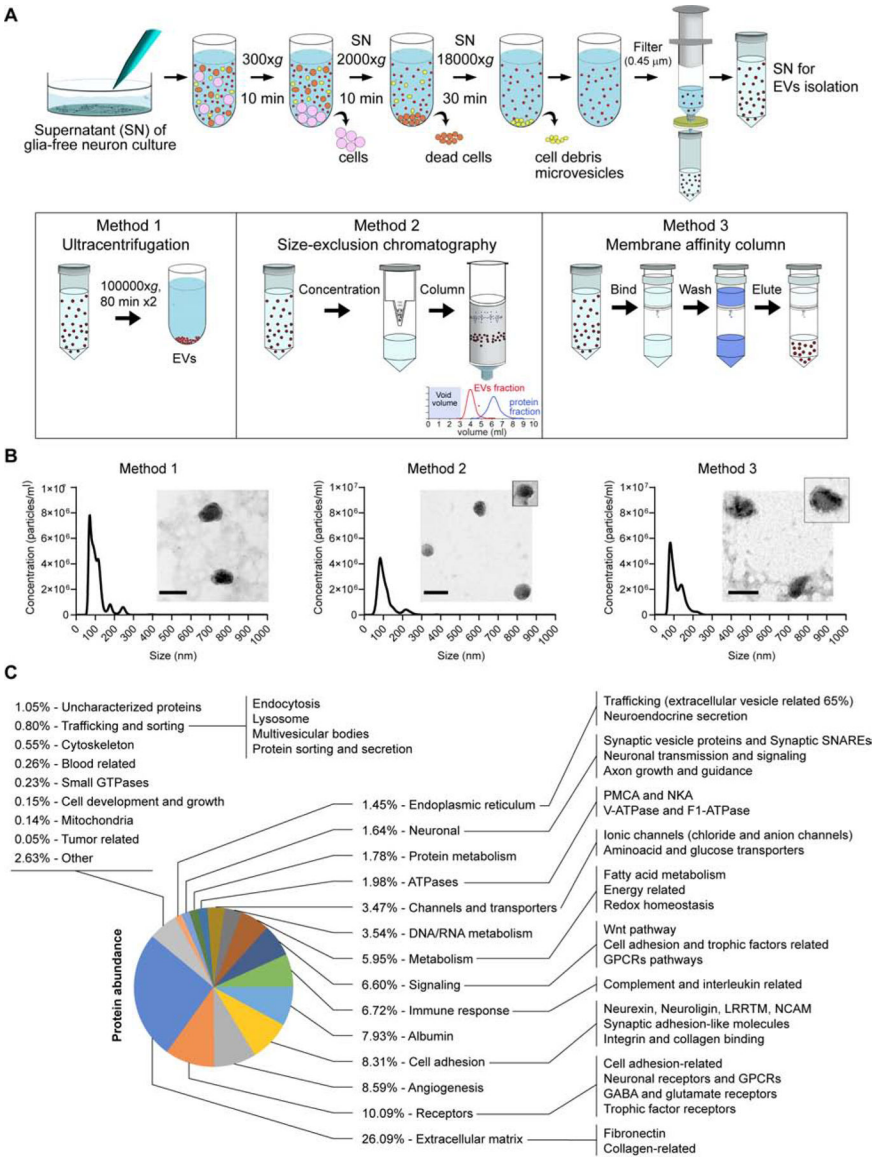

Fig. 1. Isolation and characterization of EVs released from astrocyte-free cultured hippocampal neurons.

(**A**) Schematic representation of the EV isolation methods. First, a shared clearing procedure to remove sedimented live cells, dead cells, debris and microvesicles was performed. After filtering the supernatant through a 0.45 µm syringe filter, EVs were isolated using ultracentrifugation and two commercial kits following the manufacturer's instructions. (**B**) Representative particle size distribution graphs obtained by nanoparticle tracking analysis (NTA) measurements of EVs isolated by the 3 different methods. Insets: morphologic observation of the EVs by transmission electron microscopy. Scale bar = 100 nm. (**C**) Classification of the proteome of EVs based on gene ontology and biological function/ pathway annotations from Protein Information Resource (http://proteininformationresource.org) and Panther Classification System (http://pantherdb.org).

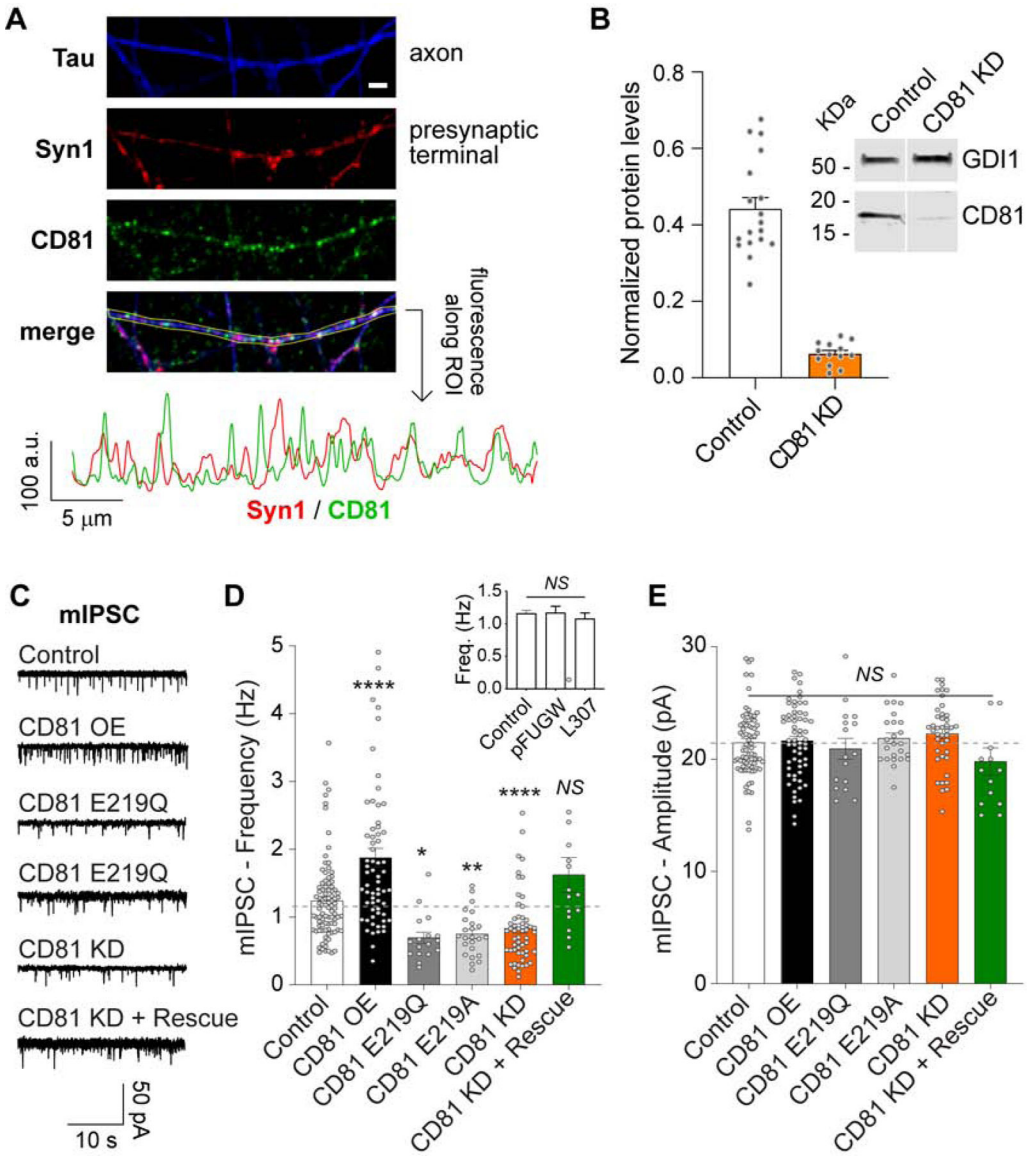

Fig. 2. Endogenous expression of CD81 by hippocampal neurons.

(**A**) Top: Representative confocal images of cultured hippocampal neurons immunofluorescently labeled with anti-synapsin 1 (red), anti-Tau (blue) and anti-CD81 (green). White scale bar = 2 µm. Bottom: fluorescence intensity quantification along the region of interest (ROI) depicted in the image. (**B**) Representative Western blot and quantification of CD81 protein levels in lysates from neurons infected with L-307 (Control) or CD81 KD lentiviruses. CD81 augments spontaneous inhibitory neurotransmission. (**C**) Representative traces, (**D**) average frequency and average amplitude (**E**) of mIPSCs in control neurons and infected with CD81, E219Q, E219A or CD81 KD lentivirus. Data was analyzed with one-way ANOVA (mIPSC frequency: $F=17.55$ $p<0.0001$ - results of the post hoc Dunnet's test are represented in the figure -; mIPSC amplitude: $F=1.449$ $p=0.2075$). Inset in D: mIPSC frequency for non-infected (control) neurons and infected with the empty vectors pFUGW and L307. One-way ANOVA: $F=0.4016$ $p=0.6703$.

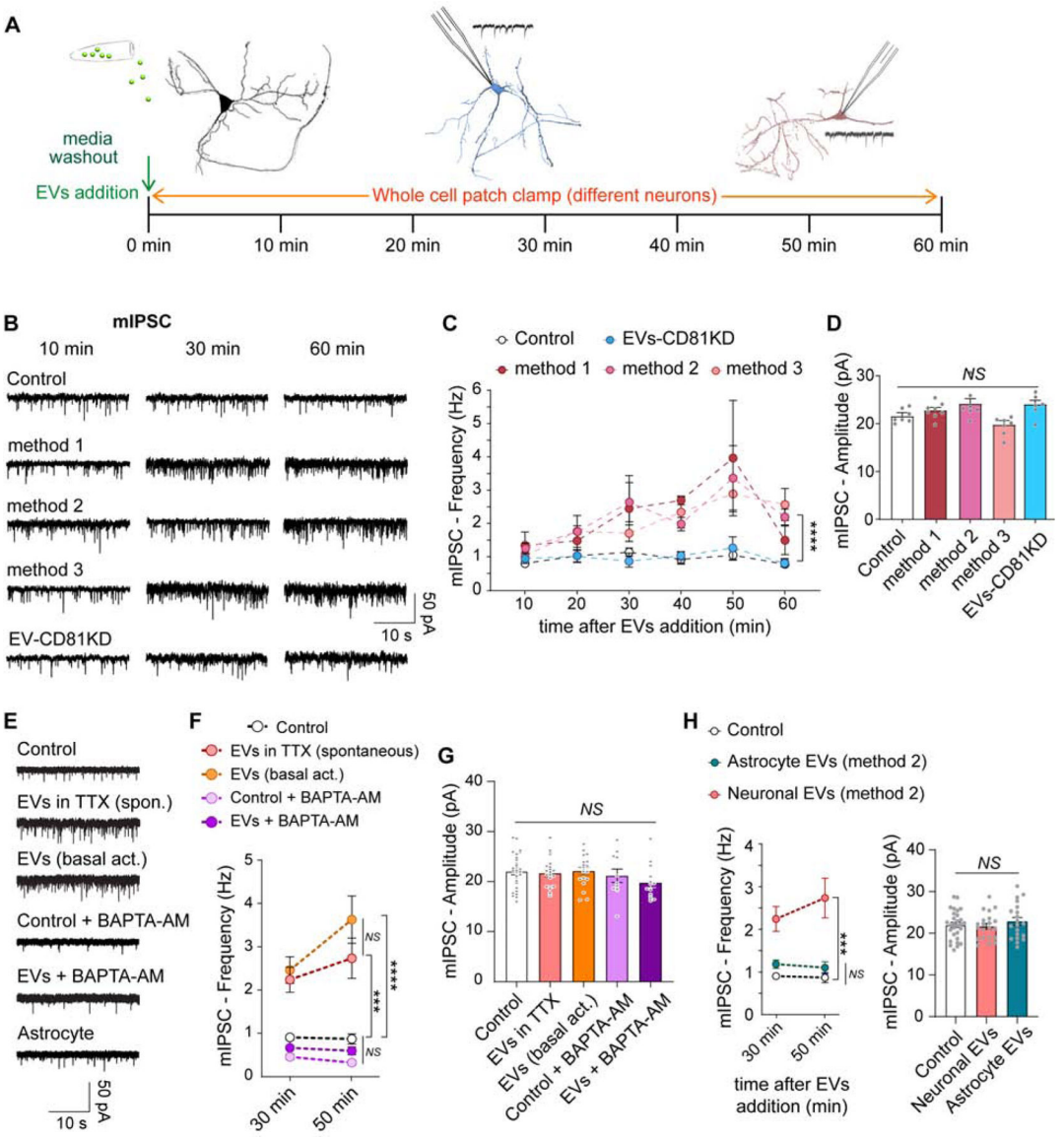

Fig. 3. Neuronal EVs containing CD81 potentiate inhibitory neurotransmission.

(**A**) Schematic representation of the experimental strategy. (**B**) Representative traces and (**C**) time course of frequency of mIPSCs in neurons incubated or not (Control) with EVs isolated by the three methods described in Fig. 1. Data was analyzed with a two-way ANOVA (time factor: $F=6.906$, $p<0.0001$; experimental group factor: $F=17.94$, $p<0.0001$). Multiple comparisons by Sidak's post hoc test revealed $p<0.0001$ (****) for all three methods vs control, and $p>0.9999$ (non-significant - NS -) for EVs CD81 KD vs control (N is 5–10 neurons per time point per group). (**D**) Average amplitudes of mIPSCs in the conditions mentioned above (two-way ANOVA: $F=0.4665$ $p=0.9749$). EV-mediated augmentation of spontaneous inhibitory neurotransmission is activity-independent and calcium-dependent. (**E**) Representative traces, (**F**) average frequency and average amplitude (**G**) of mIPSCs in neurons untreated (control) or treated with EVs in the presence (spontaneous) or absence (basal activity) of TTX. Alternatively, control or EVs groups were pretreated along with the

calcium chelator BAPTA-AM (100 μM). Data was analyzed using ANOVA (mIPSC frequency: two-way ANOVA, Group factor: $F(4,83)=33.54$ $p<0.0001$, Time factor: $F(1,83)=2.272$ $p=0.1355$ - results of the post hoc Sidak's multiple comparisons test are represented in the figure –; mIPSC amplitude: one-way ANOVA, $F=1.210$ $p=0.3124$). Astrocyte-derived EVs do not regulate mIPSC. (**H**) Neurons were preincubated in TTX alone (control) or plus EVs from neuronal or astrocytic origin. Left: Frequency of mIPSC. Right: Amplitude of mIPSC. Data was analyzed with ANOVA (mIPSC frequency: two-way ANOVA, Group factor: $F(2,64)=31.88$ $p<0.0001$, Time factor: $F(1,64)=0.5022$ $p=0.4811$; mIPSC amplitude: one-way ANOVA, $F=0.5961$ $p=0.5539$).

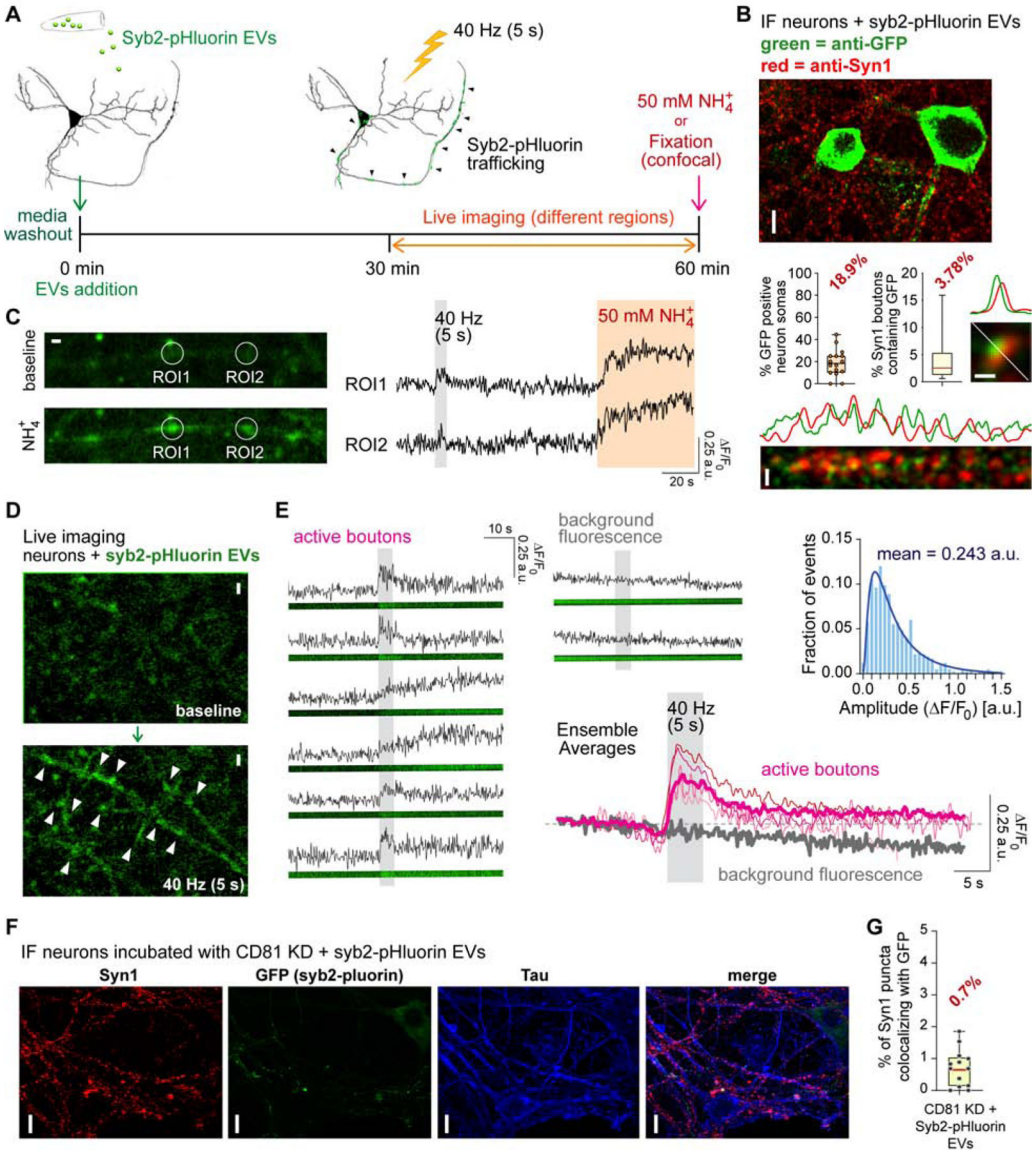

Fig. 4. Syb2 transported via EVs can be incorporated into the synaptic vesicle cycle.

(**A**) Schematic representation of the experimental strategy. (**B**) Immunofluorescence (IF) analysis of subcellular localization of GFP (to label syb2-pHluorin) and syn1. White scale bars: 10 μm for top image, 1 μm for the rest. Line scans showing similar spatial distribution for GFP and syn1 are shown. Left bar graph: quantification of the number of GFP (pHluorin) positive cell bodies relative to total neurons per image field. Right bar graph: object-based colocalization analysis and quantification of syn1 boutons containing GFP signal. (**C**) Live fluorescence imaging of syb2-pHluorin incorporated from EVs. Left: representative images of putative presynaptic boutons before and after perfusion of 50 mM NH_4Cl. Right: fluorescence traces of the two regions of interests (ROI) depicted in the images. White scale bar = 1 μm. (**D**) Representative fluorescence images of exogenous syb2-pHluorin incorporated from EVs before (top) and after (bottom) stimulation at 40 Hz for 5 s (200 AP). White scale bar = 2 μm. (**E**) Example fluorescence traces of putative presynaptic

terminals (active boutons, left) and spots of background fluorescence (top center). Center bottom: Average fluorescence traces from 4 independent experiments (thin lines; >15 recordings per experiment and >5 ROIs per recording) and ensemble average (thick lines). Inset (top right): Histogram of fluorescence amplitudes (normalized to F_0) and lognormal fit (blue line). EVs isolated from CD81 KD neurons have reduced incorporation into target WT neurons. (**F**) Representative immunofluorescence images and (**G**) object-based colocalization analysis and quantification of syn1 boutons containing GFP signal after incubation of WT neurons with EVs isolated from CD81 KD + syb2-pHluorin neuron cultures.

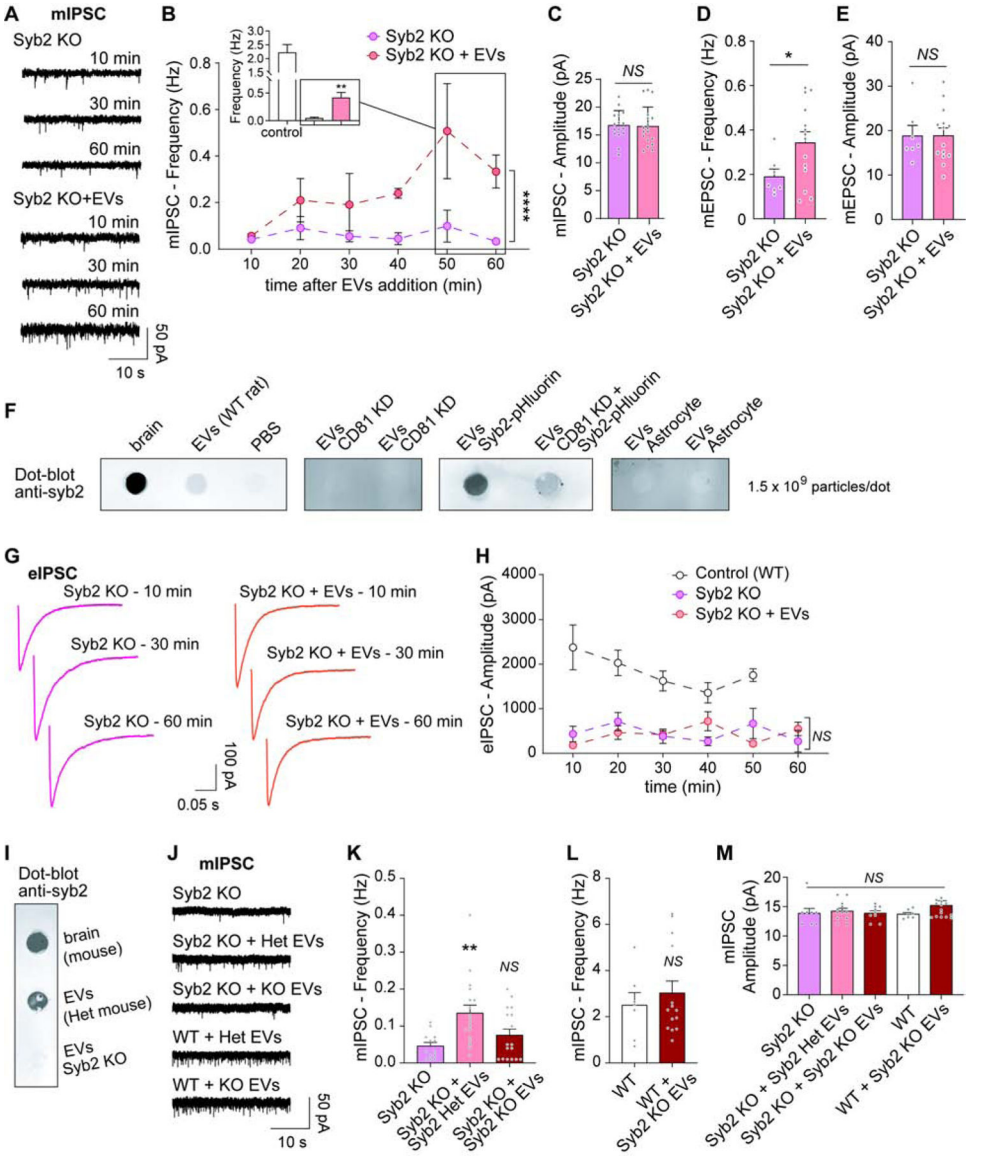

Fig. 5. Synaptobrevin-2 from EVs can rescue inhibitory and excitatory spontaneous release in Syb2 KO neurons.

(**A**) Representative traces and (**B**) time course of frequency of mIPSCs in Syb2 KO neurons incubated (Syb2 KO + EVs) or not with EVs. Two-way ANOVA: time effect F=2.575 p=0.0400, experimental group effect F=18.69 p<0.0001 (N is 4–6 neurons per time point per group). Inset: Average mIPSC frequency at 50–60 min comparing wild type (control) neurons with syb2 KO with and without EVs (syb2 KO vs syb2 KO + EVs p=0.0075 by unpaired t-test). (**C**) Average amplitude of mIPSCs in the conditions mentioned above (syb2 KO vs syb2 KO + EVs p=0.8775 by unpaired t-test). (**D**) Frequency and (**E**) Amplitude of mEPSC in Syb2 KO hippocampal neurons at 30–60 min after addition of EVs (unpaired t-test: frequency p=0.0471, amplitude p=0.9863). CD81 KD impairs Syb2 recruitment and secretion via EVs. (**F**) Dot-blot of EVs isolated from different sources, immunostained against Syb2 (whole brain lysates were used as positive controls). EVs do not increase evoked release in Syb2 KO neurons. (**G**) Representative eIPSC traces from syb2 KO neurons

incubated with or without EVs. (**H**) Time course of eIPSC amplitude after EVs addition. Two-way ANOVA: time factor F=0.9299 p=0.4474, experimental group factor F=43.79 p<0.0001 (post hoc Tukey's test revealed p<0.0001 for control vs syb2 KO and sun2 KO + EVs, p=0.7112 - NS - for syb2 KO vs syb2 KO + EVs). EVs that lack Syb2 do not modulate neurotransmission. (**I**) Dot-blot of EVs isolated from Syb2 KO neurons and their littermate controls, Syb2 heterozygous (Het; positive control = whole brain lysate). (**J**) Representative traces, (**K**–**L**) Frequency and (**M**) Amplitude of mIPSC in Syb2 KO and WT mouse hippocampal neurons incubated for 30–60 min with EVs isolated from Syb2 KO or Het neuron cultures. Data was analyzed with one-way ANOVA (mIPSC frequency in Syb2 KO: F=6.388 p=0.0036; mIPSC frequency in WT: unpaired t-test p=0.5356; mIPSC amplitude: F=0.9418 p=0.4484).

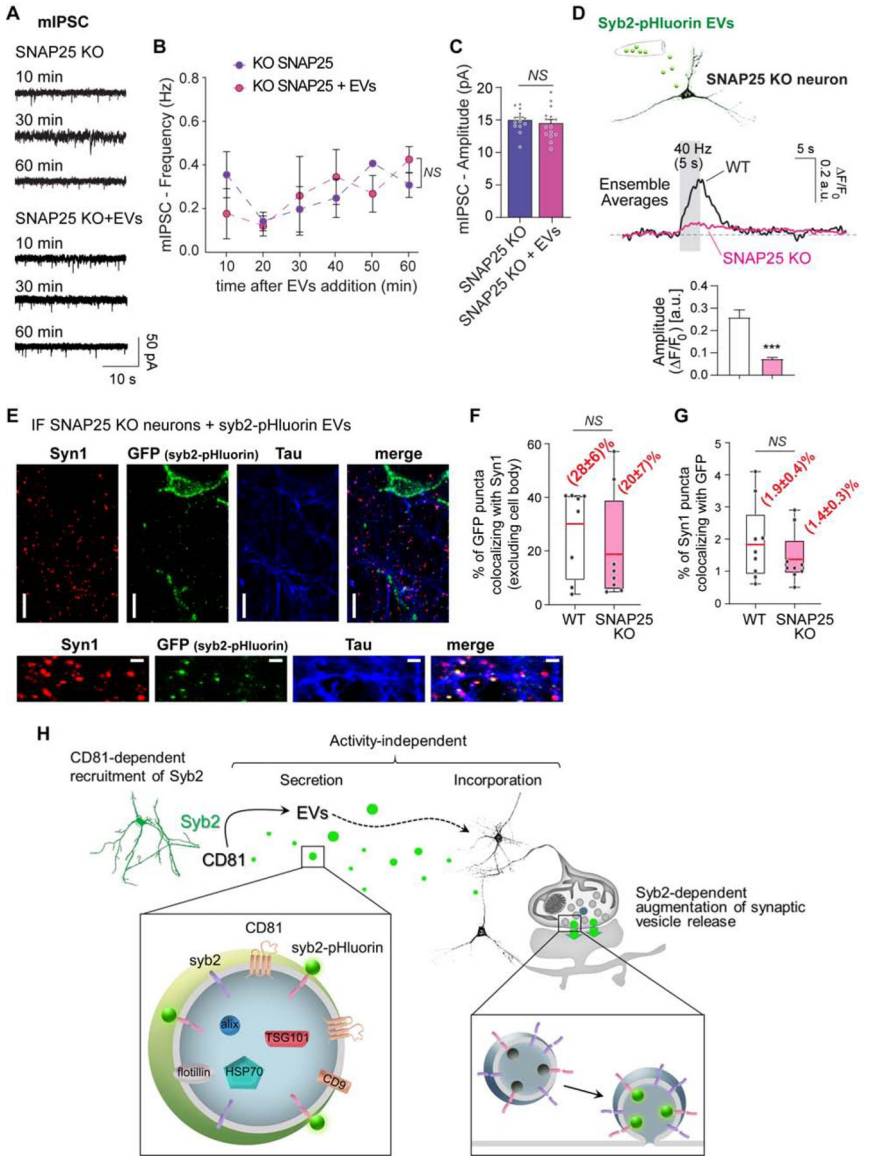

Figure 6. EVs cannot rescue spontaneous neurotransmission in SNAP25 KO neurons.

(**A**) Representative traces and (**B**) time course of frequency of mIPSCs in SNAP25 KO neurons incubated (SNAP25 KO + EVs) or not with EVs. Two-way ANOVA: time effect F=1.304 p=0.3017, experimental group effect F=0.02381 p=0.8789 (N is 3–4 neurons per time point per group). (**C**) Average amplitude of mIPSCs in the conditions mentioned above (SNAP25 KO vs SNAP25 KO + EVs p=0.8900 by unpaired t-test). (**D**). Top: Schematic representation of the experiment. Center: Average fluorescence traces in SNAP25 KO neurons and littermate control - WT - (2 independent experiments, 8–12 recordings per experiment and >5 ROIs per recording). Bottom: Fluorescence amplitudes (normalized to F0). (**E**) Representative immunofluorescence images of SNAP25 KO neurons incubated with Syb2-pHluorin EVs and immunostained against GFP, Syn1 and Tau. (**F**) Object-based colocalization analysis and quantification of fraction of GFP-positive (syb2-pHluorin) bouton-like objects colocalizing to presynaptic terminals (syn1). (**G**) Object-based

colocalization analysis and quantification of Syn1 boutons containing GFP signal after incubation of SNAP25 KO neurons with EVs syb2-pHluorin neuron cultures. (**H**) Schematic representation of the mechanism of EVs-mediated augmentation of spontaneous neurotransmission: CD81 participates in the recruitment of Syb2 to EVs for posterior secretion. EVs are then incorporated by the target neuron and the exogenous Syb2 can be functionally integrated into synaptic vesicles increasing their propensity to release.

KEY RESOURCES TABLE

REAGENT or RESOURCE	SOURCE	IDENTIFIER
Antibodies		
Guinea pig polyclonal anti-Tau	Synaptic Systems	Catalog # 314 004
Rabbit monoclonal anti-Flotilin	abcam	Catalog # EPR6041
Mouse monoclonal anti-Rab-GDI1	Synaptic Systems	Catalog # 130 011
Mouse monoclonal anti-GFAP	abcam	Catalog # ab10062
Rabbit recombinant monoclonal anti-CD81	abcam	Catalog # EPR4244
Mouse monoclonal anti-CD81	Invitrogen	Catalog # MA5-13548
Mouse monoclonal anti-CD63	abcam	Catalog # ab108950
Rabbit polyclonal anti-Synapsin1	Synaptic Systems	Catalog # 106 103
Mouse monoclonal anti-Synapsin1	Synaptic Systems	Catalog # 106 011
Mouse monoclonal anti-GFP	Cell Signaling	Catalog # 29565
Chemicals, Peptides, and Recombinant Proteins		
D(−)-2-Amino-5-phosphonopentanoic acid (AP-5)	Sigma-Aldrich	Catalog # A8054
Tetrodotoxin (TTX)	Enzo Life Sciences	Catalog # BML-NA120-0001
Picrotoxin (PTX)	Sigma-Aldrich	Catalog # P1675
6-cyano-7-nitroquinoxaline-2,3-dione (CNQX)	Sigma-Aldrich	Catalog # C239-100MG
Trypsin from bovine pancreas	Sigma-Aldrich	Catalog # T9935
DNAse	Sigma-Aldrich	Catalog # D5025-375KU
Matrigel	Corning	Catalog # 354234
FuGENE 6	Promega	Catalog # E2692
QX-314	EMD-Millipore	Catalog # 552233
Experimental Models: Cell Lines		
Highly transfectable derivative of human embryonic kidney-293 epithelial adherent cells (HEK293T)	ATCC	Catalog # CRL-1573
Experimental Models: Organisms/Strains		
Synaptobrevin 2 mice pups (embryonic)	(Schoch et al., 2001)	N/A
SNAP25 2 mice pups (embryonic)	(Bronk et al., 2007)	N/A
Sprague-Dawley rat pups (P0–P1)	Charles River	N/A
Recombinant DNA		
Plasmid: pCMV-VSV-G (lentiviral packaging)	Stewart et al., 2003	AddGene # 8454
Plasmid: pRSV-REV (lentiviral packaging)	Dull et al., 1998	AddGene # 12253
Plasmid: pMDLg/pRRE (lentiviral packaging)	Dull et al., 1998	AddGene # 12251
Plasmid: pFUGW-Synaptobrevin2-pHluorin	(Ramirez et al., 2012)	N/A
Plasmid: L307-GFP-CD81 KD shRNA	This manuscript	N/A
Plasmid: L307-CD81 KD shRNA	This manuscript	N/A
Plasmid: pFUGW-pHluorin-CD63	(Sung et al., 2015)	N/A
Plasmid: pFUGW-CD81	This manuscript	N/A
Plasmid: mCherry-CD81	Michael Davidson Lab *(not published)*	AddGene # 55012

REAGENT or RESOURCE	SOURCE	IDENTIFIER
Plasmid: pFUGW-pHluorin-CD81	This manuscript	N/A
Plasmid: pFUGW-E219A CD81	This manuscript	N/A
Plasmid: pFUGW-E219Q CD81	This manuscript	N/A
Plasmid: pFUGW-ratCD81	This manuscript	N/A
Plasmid: pFUGW-mCherry -ratCD81	This manuscript	N/A
CD81 (NM_013087) Rat Untagged Clone	ORIGENE	RN202464
Software and Algorithms		
Matlab script for pHluorin analysis	(Chanaday and Kavalali, 2018)	https://github.com/nchanaday/Single-vesicle-fusion-events
Fiji	(Schindelin et al., 2012)	N/A
GelAnalyzer 2010a	http://www.gelanalyzer.com/	N/A
Other		
commercial kit Q5® Site-Directed Mutagenesis Kit	NEB	#E0554S
qEVoriginal / 35nm - 5 Pack Remove	IZON	N/A
exoEasy Maxi Kit	QIAGEN	#76064